ICAS-98-7,9,1

A98-31718

INVESTIGATION INTO THE FORMATION OF WAVES ON THIN LAYERS OF DE-/ANTI-ICING FLUIDS ON WINGS

O.J. Boelens * and J.C. Sijp †
University of Twente, STW
Enschede, The Netherlands

Abstract: Due to the formation of waves on de-/anti-icing fluids used to protect an aircraft during take-off in winter conditions, the aircraft experiences a lift loss, a drag increase and a decrease of stall angle. The formation of these waves has been investigated by many authors using a temporal stability analysis. In this local analysis, it is assumed that the primary flow is parallel or weakly non-parallel. In case of the flow over a thin layer of liquid, however, the assumption of a parallel primary flow no longer holds. To include the effect of a non-parallel primary flow the analysis employing the one-layer Parabolized Stability Equations(PSE) has been extended to a two-layer analysis. As the PSE method is a spatial type of stability method, the stability characteristics of the flow of a gas over a thin layer of liquid have been investigated also using a local spatial stability analysis. The different modes previously observed in the temporal stability analysis, i.e. the Tollmien-Schlichting mode and the interfacial mode, are also observed in the spatial domain. The interfacial mode, characterized in the temporal domain by small growing rates, is the dominant mode(highest growing rates) in the spatial domain. The results of the local spatial stability analysis have been compared with the results obtained by applying the Gaster transformation to the results of a local temporal stability analysis. For the interfacial mode a modified Gaster transformation is introduced. The evolution of the modes in the streamwise direction has been calculated employing the two-layer PSE method. The effect of the non-parallel primary flow was found to be small. The link to experimental results has been indicated by introducing a growth rate based on the disturbance height of the interface.

1 Introduction

Two-phase flows are often encountered phenomena in every-day life. A subset of the two-phase flows are the two-layer flows. These flows are characterized by the presence of an interface, that separates the two different inmiscible fluids. Examples of these two-layer flows can be observed in, for example, distillation columns, condensors, pipe flows and coating processes. The present interest in these two-layer flow problems stems from the application of a thin layer of de-/anti-icing fluids on wing surfaces.

To protect aircraft on the ground from ice, snow or frost accumulation, it has been general practice to use water-glycol based fluids. Two basic types of fluids are used: (a) de-icing fluids, that are in general Newtonian fluids which only remove ice, snow or frost accumulation, (b) non-Newtonian anti-icing fluids that prevent ice, snow or frost accumulation to build up over a certain period of time, the so-called holdover time. In the mid 1980's it appeared that the fluids used to de-/anti-ice an aircraft might have an adverse effect on the aircraft aerodynamics, specifically during take-off. The 1982 accident of an Air Florida Boeing 737 aircraft at the airport of Washington D.C. in moderate snow conditions, resulted in an increased interest for the application of de-/anti-icing fluids to aircraft. A series of research projects at Boeing[11],[17]-[19],[27],[28],[30] the Von Kármán Institute for Fluid Dynamics[6]-[10] Fokker[14],[15] and the Université du Québec à Chicoutimi[20],[21],[25] was carried out. In these experimental studies it was found that the presence of a thin layer of de-/anti-icing fluid results in a lift loss, a drag increase and a decrease of the stall angle. The experiments showed that during take-off, before the fluid is finally blown off the surface, the interface roughens, i.e. waves are formed.[12] In order to have a simple, cost-effective aerodynamic acceptance test for de-/anti-icing fluids in a small cooled wind tunnel, it has been accepted to substitute the upper surface of the true airfoil by a flat plate, while experiments provided the correlation between the lift loss on a three-dimensional wing and the boundary-layer momentum thickness at the trailing edge of the flat plate. The formation of waves on the interface was also observed during the flat-plate fluid-certification test runs.

As indicated by experimental results, a gas-liquid interface can become unstable if the free-stream gas velocity passes a certain threshold value. A classical method to investigate the initiation of flow instabilities is the hydrodynamic stability analysis leading to the Orr-Sommerfeld Equation. Just recently a number of articles on two-layer flows in which the dynamic behaviour of both fluids is taken into account have

*PhD. Student
†MSc. Student

been published. Miesen and Boersma[22] considered a thin liquid layer flowing down a vertical plane while sheared by a gas layer (see also[3] and[5]). A spectral method was used to compute the solution to the Orr-Sommerfeld equation. At the von Kármán Institute for Fluid Dynamics, Rumberg[26] considered an infinite flat plate covered with a thin layer of liquid sheared by a gas stream and used a shooting method to compute the stability curves. Özgen[24] extended the results of Rumberg to a non-Newtonian power-law fluid. Here the power-law was used to model the viscous behaviour of de-/anti-icing fluids. Finally, Yih[29] performed an analytical investigation into the formation of waves on a liquid of high viscosity. All these references, however, focus on the local temporal stability problem. In the present paper the stability of a thin layer of liquid sheared by a gas stream will be investigated from a spatial stability point of view.
The one-layer Parabolized Stability Equations(PSE) method has been developed by Bertolotti[1] and Herbert[16] to investigate the spatial evolution of an instability. An advantage of the PSE method over local methods is that the primary flow no longer has to be parallel. In the present investigation the one-layer PSE method will be extended to a two-layer PSE method. However, before treating this problem, the one-layer Parabolized Stability Equations will be discussed and some results of the two-layer local spatial stability method are presented, see also[4] The local spatial stability results for the two-layer system were obtained by using a two-layer local spatial stability method as well as using the Gaster transformation (or the Modified Gaster transformation) applied to two-layer local temporal stability results.

2 One-layer Parabolized Stability Equations

Since long local stability analysis has been used as a tool to investigate the initiation of instabilities in a flow. The disadvantage of such a local method is that it is restricted to parallel or nearly-parallel primary flows. To overcome this disadvantage the method of the Parabolized Stability Equations(PSE) was developed, see[1] and[16] The method was used to predict instability as well as transition of the flow over aerodynamic surfaces. In the present paper the linear PSE method will be extended to the situation of a gas flowing over a flat plate covered with a thin layer of liquid, e.g. water or de-/anti-icing fluid. Before discussing this new two-layer PSE method the conventional one-layer PSE method will be described first. At the end of this chapter the results obtained by the present method will be compared with the results available in the literature.

2.1 The Governing Equations

The flow configuration is the well-known flow of a fluid over a flat plate.
Starting point for the derivation of the Parabolized Stability Equations is the two-dimensional incompressible flow of a Newtonian fluid, of constant viscosity, governed by the Navier-Stokes Equations in a Cartesian coordinate system, i.e.

$$\nabla \cdot \mathbf{v} = 0 \tag{2.1}$$

$$\frac{\partial \mathbf{v}}{\partial t} + (\mathbf{v} \cdot \nabla)\mathbf{v} = \mathbf{g} - \frac{1}{\rho}\nabla p + \frac{\mu}{\rho}\nabla^2 \mathbf{v} \tag{2.2}$$

where p is the pressure, $\mathbf{v} = (u, v)$ is the velocity vector, ρ is the density, μ is the dynamic viscosity and $\mathbf{g}$ is the gravitational acceleration vector.
Upon decomposing the flow field $\mathbf{v} = (u, v), p$ into a laminar primary flow $\mathbf{V} = (U, V), P$ and a perturbation, i.e. secondary flow, $\mathbf{v}' = (u', v'), p'$ according to

$$\mathbf{v}(x, y, t) = \mathbf{V}(x, y, t) + \mathbf{v}'(x, y, t) \tag{2.3}$$

$$p(x, y, t) = P(x, y, t) + p'(x, y, t) \tag{2.4}$$

and neglecting the terms non-linear in the secondary flow components, one obtains as leading-order terms the Navier-Stokes equations for the primary flow and as first-order terms the so-called 'linear stability equations' that govern the secondary flow, i.e.

$$\nabla \cdot \mathbf{v}' = 0 \tag{2.5}$$

$$\frac{\partial \mathbf{v}'}{\partial t} + (\mathbf{v}' \cdot \nabla)\mathbf{V} + (\mathbf{V} \cdot \nabla)\mathbf{v}' = -\frac{1}{\rho}\nabla p' + \frac{\mu}{\rho}\nabla^2 \mathbf{v}' \tag{2.6}$$

The continuity equation can be eliminated by the introduction of a stream function $\psi'(x, y, t)$ according to

$$\mathbf{v}'(x, y, t) = \begin{pmatrix} \frac{\partial}{\partial y} \\ -\frac{\partial}{\partial x} \end{pmatrix} \psi'(x, y, t) \tag{2.7}$$

Substituting this definition into the momentum equation results in the following set of equations

$$\frac{\partial^2 \psi'}{\partial t \partial y} + U\frac{\partial^2 \psi'}{\partial x \partial y} + \frac{\partial U}{\partial x}\frac{\partial \psi'}{\partial y} + V\frac{\partial^2 \psi'}{\partial y^2} - \frac{\partial U}{\partial y}\frac{\partial \psi'}{\partial x} + \frac{1}{\rho}\frac{\partial p'}{\partial x} - \frac{\mu}{\rho}\frac{\partial^3 \psi'}{\partial^2 x \partial y} - \frac{\mu}{\rho}\frac{\partial^3 \psi'}{\partial y^3} = 0 \tag{2.8}$$

$$-\frac{\partial^2 \psi'}{\partial t \partial x} - U\frac{\partial^2 \psi'}{\partial x^2} + \frac{\partial V}{\partial x}\frac{\partial \psi'}{\partial y} - V\frac{\partial^2 \psi'}{\partial x \partial y} - \frac{\partial V}{\partial y}\frac{\partial \psi'}{\partial x} + \frac{1}{\rho}\frac{\partial p'}{\partial y} + \frac{\mu}{\rho}\frac{\partial^3 \psi'}{\partial x^3} + \frac{\mu}{\rho}\frac{\partial^3 \psi'}{\partial x \partial y^2} = 0 \tag{2.9}$$

It is assumed that the secondary flow components ψ', p' can be expanded in a Fourier series, in other

words can be represented by a sum of Fourier modes. In the conventional local stability analysis, where it is assumed that the primary flow is strictly parallel, these normal modes are assumed to be of the form

$$\psi'(x,y,t) = \phi(y)e^{i(\alpha x-\omega t)} \tag{2.10}$$
$$p'(x,y,t) = f(y)e^{i(\alpha x-\omega t)} \tag{2.11}$$

where $\phi(y)$ and $f(y)$ are amplitude functions, which depend only on the coordinate normal to the surface, α is the complex wave number and ω is the complex frequency, both independent of x and t.
To include the effect of non-parallelism in the PSE analysis a different approach is taken. It is assumed that the normal modes can be decomposed according

$$\psi'(x,y,t) = \phi(x,y)\chi(x,t) \tag{2.12}$$
$$p'(x,y,t) = f(x,y)\chi(x,t) \tag{2.13}$$

where

$$\chi(x,t) = e^{i\theta(x)-i\omega t}, \frac{d\theta(x)}{dx} = \alpha(x) \tag{2.14}$$

According to Bertolotti[1] this decomposition is appropriate when the flow has the following properties

1 The velocity profiles, wavelengths, and growth rates change slowly in the streamwise direction

2 The disturbances grow and decay as convected instabilities (see[16])

The first property implies that second and higher derivatives in the streamwise direction as well as products of first derivatives may be neglected. Using this approximation one obtains, upon introducing the above decomposition, the so-called **Parabolized Stability Equations**

$$(M_0 + M_1)\mathbf{q} + M_2\frac{\partial \mathbf{q}}{\partial x} + \frac{da}{dx}M_3\mathbf{q} = \mathbf{0} \tag{2.15}$$

where $a(x) = i\alpha(x)$ and $\mathbf{q}(x,y) = (\phi(x,y), f(x,y))$. This particular formulation of the Parabolized Stability Equations is chosen to simplify the derivation of the two-layer Parabolized Stability Equation, especially the interface conditions, see chapter 4.
The operators $M_j(a,\omega,U,V)$, $j = 0(1)3$, in equation (2.15) are

$$M_0 = \begin{bmatrix} -a\frac{\partial U}{\partial y} + (aU - i\omega - \frac{\mu}{\rho}a^2)\frac{\partial}{\partial y} - \frac{\mu}{\rho}\frac{\partial^3}{\partial y^3} & \frac{a}{\rho} \\ (a^2U - i\omega a - \frac{\mu}{\rho}a^3) - \frac{\mu}{\rho}a\frac{\partial^2}{\partial y^2} & -\frac{1}{\rho}\frac{\partial}{\partial y} \end{bmatrix} \tag{2.16}$$

$$M_1 = \begin{bmatrix} \frac{\partial U}{\partial x}\frac{\partial}{\partial y} + V\frac{\partial^2}{\partial y^2} & 0 \\ a\frac{\partial V}{\partial y} + aV\frac{\partial}{\partial y} & 0 \end{bmatrix} \tag{2.17}$$

$$M_2 = \begin{bmatrix} -\frac{\partial U}{\partial y} + (U - 2\frac{\mu}{\rho}a)\frac{\partial}{\partial y} & \frac{1}{\rho} \\ (2aU - i\omega + \frac{\partial V}{\partial y} - 3\frac{\mu}{\rho}a^2) + V\frac{\partial}{\partial y} - \frac{\mu}{\rho}\frac{\partial^2}{\partial y^2} & 0 \end{bmatrix} \tag{2.18}$$

$$M_3 = \begin{bmatrix} -\frac{\mu}{\rho}\frac{\partial}{\partial y} & 0 \\ U - 3\frac{\mu}{\rho}a & 0 \end{bmatrix} \tag{2.19}$$

The system $M_0\mathbf{q} = \mathbf{0}$ represents the case of a strictly parallel primay flow, and thus is equivalent to the system that is obtained in the local stability analysis. Matrix M_1 contains the effects of the non-parallelism of the primary flow. Matrix M_2 accounts for the streamwise variation of the amplitude functions. Matrix M_3 is a consequence of the streamwise variation of the wave number.
Decomposition (2.12)-(2.13) used in the derivation of the Parabolized Stability Equations is ambiguous, i.e. both the amplitude functions and $\chi(x,t)$ depend on the streamwise coordinate x. To resolve this ambiguity the following normalization condition(see[16]) is introduced

$$\int_\Omega \frac{\partial \mathbf{q}}{\partial x} \cdot \mathbf{q}^\dagger dy = 0 \tag{2.20}$$

Here $\mathbf{q}^\dagger$ represents the complex conjugate of $\mathbf{q}$ and Ω is the integration domain in the direction normal to the solid wall. This normalization condition minimizes the streamwise changes of the amplitude function and the wavenumber α. Alternative normalization conditions can be found in the literature, e.g.[1] and[16]
The Parabolized Stability Equations constitute an initial boundary-value problem. To complete the formulation of the Parabolized Stability Equations both an initial condition and boundary conditions are needed. The initial condition is obtained by solving the local spatial stability problem, i.e. $M_0\mathbf{q} = 0$ in the above formulation. More details on the local spatial stability problem for two layers can be found in[3] The method described in[3] utilizes a virtual interface in the gas boundary layer (see also[22]) and solves the Orr-Sommerfeld equation for the amplitude function $\phi(y)$ (the pressure term is eliminated from the formulation). Once $\phi(y)$ is known the pressure amplitude function, $f(y)$, can be determined using

$$f = \left[\rho\frac{\partial U}{\partial y} + \left(\rho\left(\frac{i\omega}{a} - U\right) + \mu a\right)\frac{\partial}{\partial y} + \frac{\mu}{a}\frac{\partial^3}{\partial y^3}\right]\phi \tag{2.21}$$

Two sets of boundary conditions must be supplied to complete the formulation of the Parabolized Stability Equations. At the solid wall, the no-slip condition has to be satisfied, i.e.

$$\left.\begin{array}{l}\phi(x,y)=0\\ \frac{\partial\phi}{\partial y}(x,y)=0\end{array}\right\} \quad \text{at} \quad y=0 \qquad (2.22)$$

The boundary conditions at infinity follow from the assumption that far away from the wall the secondary flow components die out. Thus, one obtains

$$\left.\begin{array}{l}\phi(x,y)\to 0\\ f(x,y)\to 0\end{array}\right\} \quad \text{as} \quad y\to\infty \qquad (2.23)$$

The initial boundary-value problem as described in this paragraph has to be solved numerically.

2.2 The numerical implementation

The Parabolized Stability Equations, Equation (2.15), together with the boundary conditions, Equations (2.22) and (2.23), and the normalization condition, Equation (2.20), form an eigenvalue problem in the unknown shape function $\mathbf{q}$ and wave number $a(x)$. Starting from an initial solution obtained with a local spatial stability analysis, the streamwise evolution of the shape function $\mathbf{q}$ and the wave number $a(x)$ can be calculated. All quantities are non-dimensionalized using the free-stream velocity U_∞ and the boundary-layer length scale at x_0, $L_0^* = (\nu x_0/U_\infty)^{1/2}$. In the remainder of this paper it is assumed that the solution at station x_i is known either from a local spatial stability analysis or from the procedure to calculate the solution of Parabolized Stability Equations at this station. The streamwise derivatives are approximated by backward differences, i.e.

$$\left.\frac{\partial(\cdot)}{\partial x}\right|_i = \frac{(\cdot)|_{i+1}-(\cdot)|_i}{\Delta x_i} \qquad (2.24)$$

with $\Delta x_i = x_{i+1} - x_i$. Equation (2.15) then reduces to

$$\begin{aligned}&(\Delta x_i(M_0+M_1)+M_2)\,|_{i+1}^{k}\mathbf{q}|_{i+1}^{k+1}\\ &\quad +(a_{i+1}^{k}-a_i)M_3|_{i+1}^{k}\mathbf{q}|_{i+1}^{k+1} = M_2|_{i+1}^{k}\mathbf{q}|_i \qquad (2.25)\end{aligned}$$

where k denotes the iteration number.
The equation describing the correction needed for the wave number is

$$a_{i+1}^{k+1} = a_{i+1}^{k} + \frac{1}{\Delta x_i}\frac{\int_\Omega \left(\mathbf{q}|_{i+1}^{k}-\mathbf{q}|_i\right)\cdot\mathbf{q}^\dagger|_{i+1}^{k}dy}{\int_\Omega |\mathbf{q}|_{i+1}^{k}|^2 dy} \qquad (2.26)$$

This equations provides that, once the solution is converged, i.e. $a_{i+1}^{k+1} = a_{i+1}^{k}$, the normalization condition, Equation (2.20), is satisfied.
Equation (2.25) and (2.26) only contain derivatives and integrals with respect to the normal direction. In this direction the unknown amplitude function $\mathbf{q}$ will be represented by a truncated Chebyshev expansion. The semi-infinite domain $y \in [0,\infty>$ is scaled to the finite domain $z \in [-1,1]$ using

$$z = \frac{1-\frac{y}{y^*}}{1+\frac{y}{y^*}} \qquad (2.27)$$

where y^* is a constant used to change the distribution of the grid points. The Gauss-Lobatto distribution in the z-domain is used for the collocation points. For more details see[3] The integration over the Ω-domain is carried out using the trapezoidal rule.
The resulting algebraic system for the coefficients of the Chebyshev series expansion is solved iteratively until the solution is converged†. Thereafter the procedure marches on to the next streamwise station, see Figure 1.

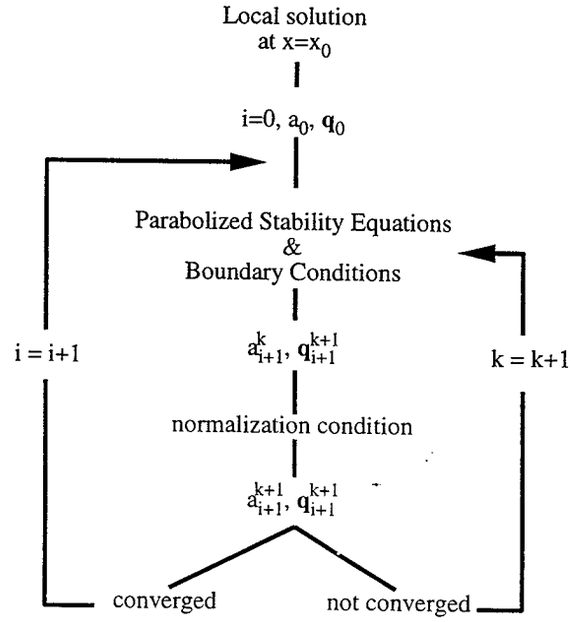

Figure 1: The numerical solution procedure

In the next paragraph results of the present method will be compared with results found in the literature, e.g.[1],[16]

2.3 Results

To validate the method described in the previous paragraphs the results for a strictly parallel boundary-layer flow and for a non-parallel boundary-layer flow given by Herbert[16] have been used for verification of the implementation.

†When the equations are solved iteratively k becomes $k+1$ in the second term on the right-hand side of Equation (2.26)

The first case considered is the strictly parallel, single-phase, boundary-layer flow. For this calculation it is assumed that the primary velocity profile(Blasius) does not change with the streamwise coordinate. The parameter values are given in Table 1 (Note the values between brackets are the non-dimensionalized frequencies, $(\omega L_0^*)/U_\infty$).

	Case (a)	Case (b)
$U_\infty[m/s]$	10	
$\nu_g[m^2/s]$	10^{-5}	
x_0 [m]	0.16	
Δx [m]	$5.0 \cdot 10^{-3}$	
no_{poly}	40	
η_{vi}	20	
y^*	10	
$\omega_0[Hz]$	860(0.0344)	430(0.0172)
$\omega[Hz]$	860(0.0344)	

Table 1: Parameter values used in boundary-layer flow test cases

In Case (b) the frequency for the initial solution is half the frequency used in the remainder of the domain. Results for these two cases are shown in Figures 2 and 3. The figures show good agreement with results of Herbert. Case (a) verifies the implementation of the PSE method. Case (b) shows, as was observed by Herbert, that even a poor initial condition leads, after a short transient region, to the most unstable mode. However, case (a) shows also a weak transient that was not observed by Herbert. This transient might be caused by the less accurate initial condition used in the present calculation. The initial condition, that Herbert uses, is calculated using a local formulation of the Parabolized Stability Equations for a non-parallel flow, whereas in our case the solution of the strictly parallel Orr-Sommerfeld equation has been used.

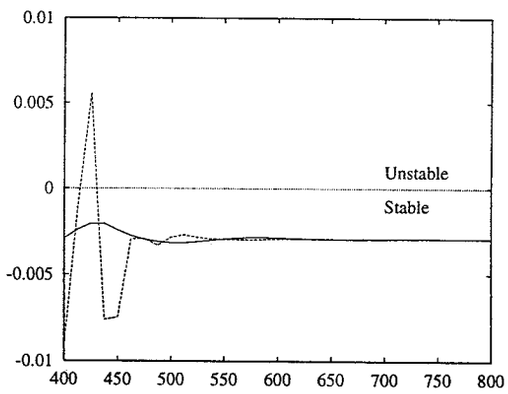

Figure 2: Strictly parallel boundary-layer flow: a_r vs. x/L_0^*; parameter values are given in Table 1; ——: Case (a), ---: Case(b)

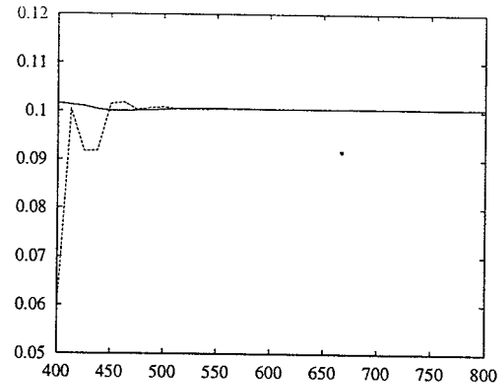

Figure 3: Strictly parallel boundary-layer flow: a_i vs. x/L_0^*; parameter values are given in Table 1; ——: Case (a), ---: Case(b)

The second case considered is the non-parallel boundary-layer flow. The parameter values used are given in Table 1, Case (a). The primary flow varies with the streamwise coordinate according to the Blasius equation. The results are shown in Figures 4, 5 and 6

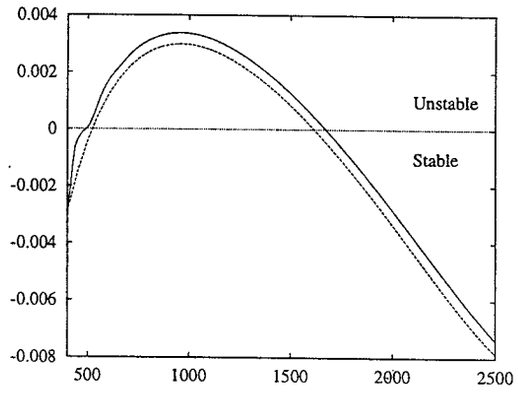

Figure 4: Non-parallel boundary-layer flow: a_r vs. x/L_0^*; parameter values are given in Table 1; ——: Parabolized Stability Equation, ---: Local Spatial Stability(Orr-Sommerfeld)

The figures show good agreement between the results obtained with the present PSE method and the method used by Herbert. As can be seen from the figures, the streamwise variation of both the wavenumber and the streamfunction, c.q. the velocity profile, is small. Therefore the effect of the non-parallel primary flow is, as previously observed by many authors, small. The problem that the growing boundary layer leaves the computational grid, as stated by Herbert, was resolved by using the transformation given in Equation (2.27). It should, however, be noted that using this transformation care should be taken to place enough points in the boundary layer close to the starting point of the PSE analysis.

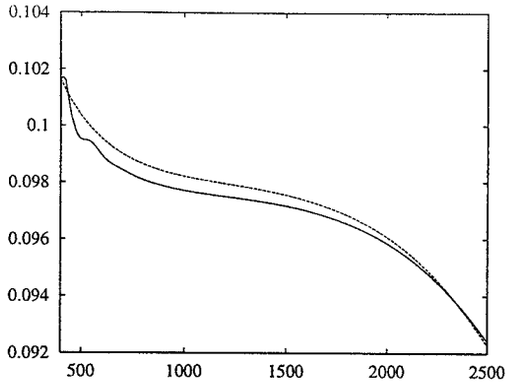

Figure 5: Non-parallel boundary-layer flow: a_i vs. x/L_0^*; parameter values are given in Table 1; ——: Parabolized Stability Equation, ---: Local Spatial Stability(Orr-Sommerfeld)

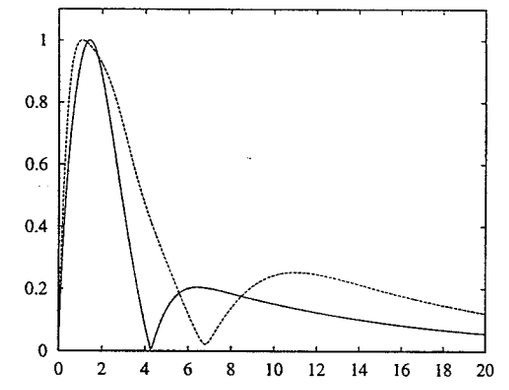

Figure 6: Non-parallel boundary-layer flow: u'/u'_{max} vs. y/L_0^*; parameter values are given in Table 1; ——: $x/L_0^* = 500$, ---: $x/L_0^* = 2000$

Before continuing with the two-layer PSE method, first a brief description will be given of the local spatial stability problem for a two-layer system. Attention will be given to the Gaster transformation in case of an interfacial mode(I-mode).

3 Two-layer local spatial stability analysis

In the literature the two-layer stability problem has received a considerable amount of attention, see[5],[22] for recent articles on this subject. These analyses, however, have been limited to the two-layer local temporal stability problem. The two-layer local spatial stability problem has not been addressed. Because the method of the Parabolized Stability Equations is a spatial stability method, some remarks will be made concerning two-layer local spatial stability methods. More details can be found in[3] and[4]

As is the case for the one-layer stability problem, the equations that govern the two-layer local spatial stability problem are the same as those that govern the two-layer local temporal stability problem. Therefore, both shooting methods and spectral methods can be used to calculate the eigenvalues and eigenfunctions. It should, however, be noted that whereas the local temporal problem is linear in the frequency ω, the local spatial stability problem is fourth order in α. The results shown in this paragraph have been calculated using a spectral method, see[3]

In the two-layer local temporal stability analysis two different modes have been observed, see[24] The first mode is the 'so-called' Tollmien-Schlichting mode and has its origin in the gas boundary layer. This mode is also present in the one-layer stability problem. In addition to this mode an interfacial mode was observed. This mode originates from the jump in viscosity, density, velocity gradient across the interface. These two modes have also been observed in the two-layer local spatial stability analysis. The appearance of the two modes in the temporal stability analysis and those inthe spatial stability analysis can, however, be different. An interfacial mode with small growth rates in the temporal case can become the dominant mode in the spatial case, and vice versa. This is illustrated in Figure 7 and 8, to be discussed shortly.

For the one-layer local stability problem Gaster[13] derived a transformation relating approximately temporal stability results to spatial stability results. In[4] this transformation is reviewed. It has been found that for the two-layer flow configuration the Gaster transformation is not valid for the interfacial mode. A Modified Gaster transformation to transform temporal results into spatial results has been introduced according to

$$\begin{aligned} \alpha_r(S) &= \alpha_r(T) \\ \alpha_i(S) &= -\omega_i(T)\left[\frac{\partial \omega_r}{\partial \alpha_r}(T)\right]^{-1} \\ \omega_r(S) &= \omega_r(T) + \underline{\omega_i(T)\left[\frac{\partial \omega_i}{\partial \alpha_r}(T)\right]\left[\frac{\partial \omega_r}{\partial \alpha_r}(T)\right]^{-1}} \end{aligned} \tag{3.1}$$

where T denotes the temporal case and S denotes the spatial case. The underlined term differentiates this transformation from the conventional Gaster transformation.

Figure 7 and 8 are representative for the situation that can be found for the flow of a gas layer over a thin layer of de-/anti-icing fluid. For a de-/anti-icing fluid the viscosity ratio $m = \mu_l/\mu_g$ can, however, still be up to 1000 times larger in magnitude than the value of 500 used in the present computation. For these liquids, the interfacial mode that for the present parameter values is much larger than the Tollmien-Schlichting mode becomes even more unstable and its maximum shifts towards lower frequencies, ω_r. A complete description of these phenomena is given in[4] In the next chapter the new method of two-layer Parabolized Stability Equations will be presented. The initial condition for the

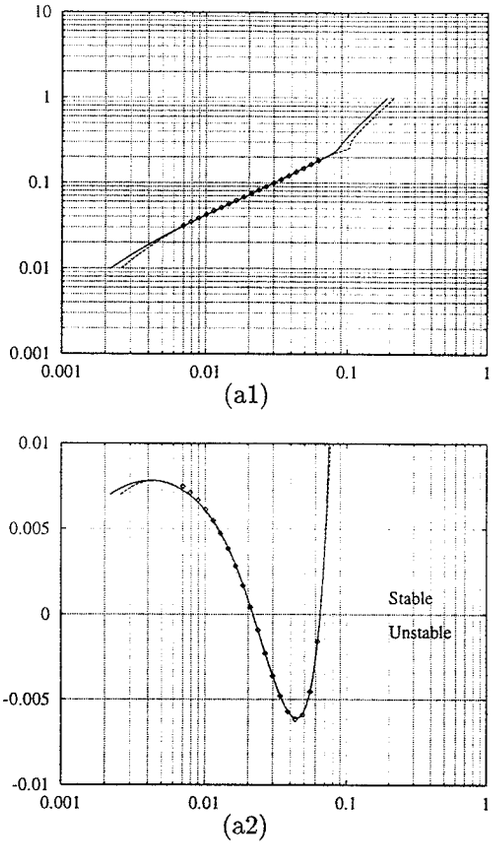

Figure 7: Two-layer local spatial stability, Tollmien-Schlichting mode: $Re = U_\infty L^*/\nu_g = 1000$, $L^* = 2.5 \cdot 10^{-4}m$, $h = 1 \cdot 10^{-3}m$, $m = \mu_l/\mu_g = 500$, $r = \rho_l/\rho_g = 1000$, $\eta_{vi} = 20$, no gravity and no surface tension; (a1) $\alpha_r(S)$ versus $\omega_r(S)$, (a2) $\alpha_i(S)$ versus $\omega_r(S)$ ——: Gaster transformation, ---: Modified Gaster transformation (Equation (3.1)), ◇: local spatial stability analysis

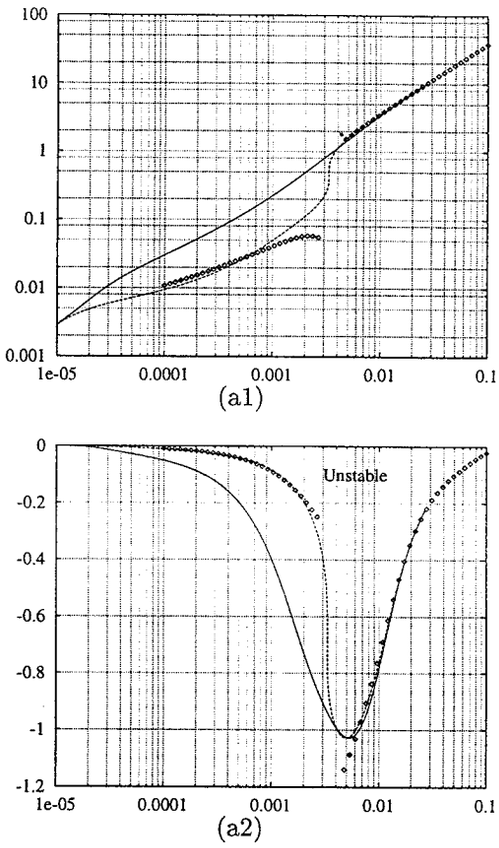

Figure 8: Two-layer local spatial stability, interfacial mode: $Re = U_\infty L^*/\nu_g = 1000$, $L^* = 2.5 \cdot 10^{-4}m$, $h = 1 \cdot 10^{-3}m$, $m = \mu_l/\mu_g = 500$, $r = \rho_l/\rho_g = 1000$, no gravity and no surface tension (see also Table 2); (a1) $\alpha_r(S)$ versus $\omega_r(S)$, (a2) $\alpha_i(S)$ versus $\omega_r(S)$;——: Gaster transformation, ---: Modified Gaster transformation (Equation3.1), ◇: local spatial stability analysis

two-layer PSE method is the result of a two-layer local spatial stability analysis. Therefore, the different modes observed for the local spatial stability analysis are also expected to appear in the results of the two-layer PSE method.

4 Two-layer Parabolized Stability Equations

In this section the new method of two-layer Parabolized Stability Equations will be derived. The method is similar to the one-layer PSE method described in section 2. Due to the introduction of the liquid layer, however, an interface and, thus in the mathematical formulation, interface conditions are introduced. The treatment of these interface conditions and the associated problems are discussed in paragraph 4.2. First the primary velocity profile is discussed.

4.1 The primary flow

The primary flow is governed by the two-dimensional incompressible Navier-Stokes equations for a Newtonian fluid in a Cartesian coordinate system, see Equations (2.1) and (2.2). The location of the interface is given by the kinematic interface condition

$$\frac{\partial h}{\partial t} + u\frac{\partial h}{\partial x} = v \quad \text{at} \quad y = h(x,t) \tag{4.1}$$

The interface conditions are

- continuity of velocity in the streamwise direction

$$[\![u(x, y = h(x,t), t)]\!] = 0 \tag{4.2}$$

- continuity of velocity in the normal direction

$$[\![v(x, y = h(x,t), t)]\!] = 0 \tag{4.3}$$

- continuity of tangential stress

$$[\![s_t(x, y = h(x,t), t)]\!] = 0 \tag{4.4}$$

- continuity of normal stress

$$[\![s_n(x, y = h(x,t), t)]\!] = -\sigma K \qquad (4.5)$$

where $[\![\cdot]\!]$ designates the jump across the interface, σ the constant surface tension $[Nm^{-1}]$ and K the local curvature of the interface$[m^{-1}]$. The components of the total stress vector s at $y = h(x,t)$ are

$$\begin{aligned} s_t \quad &= \frac{\mu}{1+\left(\frac{\partial h}{\partial x}\right)^2}\left(1-\left(\frac{\partial h}{\partial x}\right)^2\right)\left(\frac{\partial u}{\partial y}+\frac{\partial v}{\partial x}\right) \\ &+\frac{\mu}{1+\left(\frac{\partial h}{\partial x}\right)^2}2\frac{\partial h}{\partial x}\left(\frac{\partial v}{\partial y}-\frac{\partial u}{\partial x}\right) \end{aligned} \qquad (4.6)$$

and

$$\begin{aligned} s_n = -p \quad &+\frac{\mu}{1+\left(\frac{\partial h}{\partial x}\right)^2}\left(2\frac{\partial v}{\partial y}+2\left(\frac{\partial h}{\partial x}\right)^2\frac{\partial u}{\partial x}\right) \\ &-\frac{\mu}{1+\left(\frac{\partial h}{\partial x}\right)^2}2\frac{\partial h}{\partial x}\left(\frac{\partial u}{\partial y}+\frac{\partial v}{\partial x}\right) \end{aligned} \qquad (4.7)$$

Using boundary-layer theory Nelson, Alving and Joseph[23] obtained a non-similar, non-parallel, steady-flow solution for the set of equations given above. Their solution is derived for a large value of the streamwise coordinate x, and is a global attractor for all initial conditions. The equations used here to calculate the primary flow are a modification of this asymptotic solution. The liquid layer height is calculated using

$$H(x) = H_0\frac{x^{\frac{1}{4}}}{x_0^{\frac{1}{4}}} \qquad (4.8)$$

and the velocity components in the liquid layer are

$$U(x,y) = \frac{2Q}{H_0^2}\frac{y x_0^{1/2}}{x^{1/2}} \qquad V(x,y) = \frac{Q}{2H_0^2}\frac{y^2 x_0^{1/2}}{x^{3/2}} \qquad (4.9)$$

where Q is the constant volume flux(m^2/s) in the liquid layer. Note that the slope of the liquid layer height is small compared to the slope of the boundary layer thickness. The velocity profile in the gas boundary layer is calculated using the Blasius equation

$$\frac{d^3 f}{d\eta^3}+\frac{1}{2}f\frac{d^2 f}{d\eta^2} = 0 \qquad (4.10)$$

where the similarity coordinate is given by $\eta = (y - H(x))(U_\infty/(\nu_g x))^{1/2}$ and $df/d\eta = U$. The boundary conditions at the interface[‡] are $f = 0$ and $df/d\eta = (2Q/h_0)(x_0/x)^{1/4}$. At infinity the streamwise velocity component should approach the free-stream velocity, i.e. $df/d\eta \to U_\infty$. It should be noted that the asymptotic profile given by Nelson et al. only coincides with the approximation of the primary velocity profile used here for large values of the streamwise coordinate x.

[‡]Here it is used that for a steady solution the kinematic interface condition reduces to $UdH/dx = V$

4.2 The governing equations

The equations describing the two-layer Parabolized Stability Equations in the liquid layer and the ones in the gas layer are the same as those describing the single layer Parabolized Stability Equations, i.e. Equation (2.15). In the remainder of this paper the subscripts $_l$ and $_g$ are used to denote the liquid layer and the gas layer, respectively. Hence in the gas layer one has $\mu = \mu_g$ and $\rho = \rho_g$, and in the liquid layer $\mu = \mu_l$ and $\rho = \rho_l$, etc.

The derivation of the interface conditions in PSE form is similar to the derivation of the Parabolized Stability Equations. The equations are derived from the kinematic interface condition, Equation (4.1), the continuity of velocity in the streamwise direction, Equation (4.2), the continuity of velocity in the normal direction, Equation (4.3), the continuity of the tangential stress component, Equation (4.4), and the continuity of the normal stress component, Equation (4.5). The flow field is decomposed according to Equation (2.3) and (2.4). In addition to this decompostion the interface location is decomposed according to

$$h(x,t) = H(x,t) + h'(x,t) \qquad (4.11)$$

The equations governing the secondary flow have to be linearized around $y = H(x,t)$. Thereafter, the terms non-linear in the secondary flow components are neglected and a stream function according to Equation (2.7) is introduced. Finally, the normal mode expansion as given by Equations (2.12) and (2.13) is introduced, along with

$$h'(x,t) = \hat{h}(x)\chi(x,t) \qquad (4.12)$$

Using Bertolotti's assumptions (see paragraph 2.1), the following equations have been derived for the interface conditions in the the two-layer PSE method

- Kinematic interface condition

$$\begin{aligned} &U\frac{d\hat{h}}{dx}+(aU-i\omega)\hat{h} = \\ &-\frac{dH}{dx}\frac{\partial\phi}{\partial y}-\frac{\partial\phi}{\partial x}-a\phi \quad \text{at} \quad y = H(x) \end{aligned} \qquad (4.13)$$

- Continuity of velocity components across the interface

$$M_{10_g}\mathbf{q}_g + M_{12_g}\frac{\partial \mathbf{q}_g}{\partial x} + M_{10_l}\mathbf{q}_l + M_{12_l}\frac{\partial \mathbf{q}_l}{\partial x} = (E_{10} + E_{11})\hat{h} \quad \text{at} \quad y = H(x) \tag{4.14}$$

- Continuity of stress components across the interface

$$(M_{20_g} + M_{21_g})\mathbf{q}_g + M_{22_g}\frac{\partial \mathbf{q}_g}{\partial x} + \frac{da}{dx}M_{23_g}\mathbf{q}_g + (M_{20_l} + M_{21_l})\mathbf{q}_l + M_{22_l}\frac{\partial \mathbf{q}_l}{\partial x} + \frac{da}{dx}M_{23_l}\mathbf{q}_l = = (E_{20} + E_{21})\hat{h} + E_{22}\frac{d\hat{h}}{dx} + \frac{da}{dx}E_{23}\hat{h} \quad \text{at} \quad y = H(x) \tag{4.15}$$

The operators in the above expressions are given in Appendix I. The representation of the problem in both the amplitude functions $\phi(x,y)$ and $f(x,y)$ is for the two-layer Parabolized Stability Equations necessary, because due to the presence of the derivative of $f(x,y)$ with respect to the streamwise coordinate x the pressure can not be eliminated from the interface conditions. The observations in paragraph 2.1 with respect to the ambiguity of the decomposition still hold. Therefore in the two-layer case the normalization condition, Equation (2.20), is once more incorporated in the model.
To close the system both boundary conditions and an initial condition are needed. The solid-wall boundary condition for the liquid layer and the free-stream condition in the gas layer equal those for the single-layer case, see Equation (2.22) with subscript $_l$ and Equation (2.23) with subscript $_g$, respectively. The initial condition is obtained by solving the local spatial stability problem for the two-layer case, see chapter 3 and[3] The problem of the unknown pressure amplitude function is solved as described in paragraph 2.1.

4.3 The numerical implementation

The numerical implementation of the equations for the two-layer system derived in the previous paragraph is similar to the one described for the single-layer problem, see paragraph 2.2. Due to the variation of the liquid-layer height in streamwise direction, the location of the collocation points in the normal direction will, however, vary with the streamwise location. Therefore, the streamwise derivatives have to be calculated in a slightly different manner. In addition to the Cartesian (x,y) coordinate system a non-orthogonal (ξ,η) coordinate system has been introduced, see Figure 9.

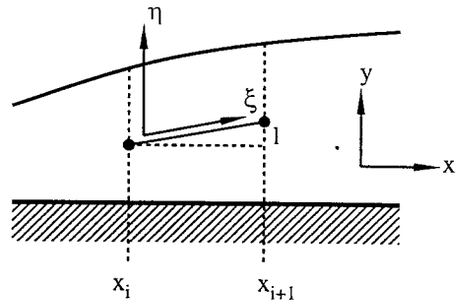

Figure 9: The Cartesian and non-orhogonal coordinate system

Here ξ is the direction coinciding with the line connecting two points with the same z-coordinate, Equation (2.27), and η coincides with the surface-normal direction. Using Bertolotti's first assumption (see paragraph 2.1), i.e. assuming that second and higher derivatives of the interface height in the streamwise direction and products of first derivatives in that direction may be neglected [§], it is easy to derive that

$$\frac{\partial}{\partial x} = \frac{\partial}{\partial \xi} - \frac{dl}{dx}\frac{\partial}{\partial \eta} \tag{4.16}$$

$$\frac{\partial}{\partial y} = \frac{\partial}{\partial \eta} \tag{4.17}$$

and

$$\Delta\xi = \Delta x \tag{4.18}$$

$$\Delta\eta = \Delta y - \frac{dl}{dx}\Delta x \tag{4.19}$$

It should be noted that at the interface dl/dx reduces to dH/dx.
Using this coordinate transformation the Parabolized Stability Equations in both the liquid layer and the gas layer become

$$(M_0 + M_1)\mathbf{q} + M_2\left[\frac{\partial \mathbf{q}}{\partial \xi} - \frac{dl}{dx}\frac{\partial \mathbf{q}}{\partial y}\right] + \frac{da}{dx}M_3\mathbf{q} = 0 \tag{4.20}$$

The kinematic interface condition is simplified to

$$U\frac{d\hat{h}}{d\xi} + (aU - i\omega)\hat{h} + \frac{\partial \phi}{\partial \xi} + a\phi = 0 \quad \text{at} \quad y = H(x) \tag{4.21}$$

For the continuity of velocity components across the interface, one obtains

[§] Consistent with the primary flow derivation in paragraph 4.1 this is a legitimate assumption, because the variation of the liquid layer height is small compared to the variation of the boundary-layer thickness

$$M_{10_g}\mathbf{q}_g + M_{12_g}\left[\frac{\partial \mathbf{q}_g}{\partial \xi} - \frac{dH}{dx}\frac{\partial \mathbf{q}_g}{\partial y}\right] + M_{10_l}\mathbf{q}_l + M_{12_l}\left[\frac{\partial \mathbf{q}_l}{\partial \xi} - \frac{dH}{dx}\frac{\partial \mathbf{q}_l}{\partial y}\right] = (E_{10} + E_{11})\hat{h} \quad \text{at} \quad y = H(x) \tag{4.22}$$

and for the continuity of stress components across the interface one finds

$$(M_{20_g} + M_{21_g})\mathbf{q}_g + M_{22_g}\left[\frac{\partial \mathbf{q}_g}{\partial \xi} - \frac{dH}{dx}\frac{\partial \mathbf{q}_g}{\partial y}\right] + \frac{da}{dx}M_{23_g}\mathbf{q}_g + (M_{20_l} + M_{21_l})\mathbf{q}_l + M_{22_l}\left[\frac{\partial \mathbf{q}_l}{\partial \xi} - \frac{dH}{dx}\frac{\partial \mathbf{q}_l}{\partial y}\right] + \frac{da}{dx}M_{23_l}\mathbf{q}_l = (E_{20} + E_{21})\hat{h} + E_{22}\frac{d\hat{h}}{d\xi} + \frac{da}{dx}E_{23}\hat{h} \quad \text{at} \quad y = H(x) \tag{4.23}$$

The Parabolized Stability Equations, the boundary and interface conditions, and the normalization condition once more form an eigenvalue problem providing the wave number $a(x)$ as well as the unknown shape functions $\mathbf{q}_l$ and $\mathbf{q}_g$ and the disturbance height $\hat{h}$. Upon discretizing the governing equations the evolution of the amplitude functions, the disturbance height as well as the wave number can be calculated.
Using Equation (4.18) the Parabolized Stability Equations in both the gas layer and the liquid layer reduce to

$$\left(\Delta x_i(M_0 + M_1) + \left(1 - \Delta x_i\frac{dl}{dx}\frac{\partial}{\partial y}\right)M_2\right)|_{i+1}^{k}\mathbf{q}|_{i+1}^{k+1} + (a_{i+1}^{k} - a_i)M_3|_{i+1}^{k}\mathbf{q}|_{i+1}^{k+1} = M_2|_{i+1}^{k}\mathbf{q}|_i \tag{4.24}$$

The kinematic interface condition in its discretized form becomes

$$\left(U|_{i+1}^{k} + \Delta x_i(aU - i\omega)|_{i+1}^{k}\right)\hat{h}|_{i+1}^{k+1} + (1 + \Delta x_i)|_{i+1}^{k}\phi_{i+1}^{k+1} = U|_{i+1}^{k}\hat{h}|_i + \phi|_i \tag{4.25}$$

The discretization of the interface conditions results in

$$\begin{aligned}
&\Delta x_i M_{10_g}|_{i+1}^{k}\mathbf{q}_g|_{i+1}^{k+1} \\
&+ \left(1 - \Delta x_i\frac{dH}{dx}\frac{\partial}{\partial y}\right)M_{12_g}|_{i+1}^{k}\mathbf{q}_g|_{i+1}^{k+1} \\
&+ \Delta x_i M_{10_l}|_{i+1}^{k}\mathbf{q}_l|_{i+1}^{k+1} \\
&+ \left(1 - \Delta x_i\frac{dH}{dx}\frac{\partial}{\partial y}\right)M_{12_l}|_{i+1}^{k}\mathbf{q}_l|_{i+1}^{k+1} \\
&- \Delta x_i\,(E_{10} + E_{11})\,|_{i+1}^{k}\hat{h}|_{i+1}^{k+1} = \\
&= M_{12_g}|_{i+1}^{k}\mathbf{q}_g|_i + M_{12_l}|_{i+1}^{k}\mathbf{q}_l|_i \quad \text{at} \quad y = H(x)
\end{aligned} \tag{4.26}$$

and

$$\begin{aligned}
&\Delta x_i(M_{20_g} + M_{21_g})|_{i+1}^{k}\mathbf{q}_g|_{i+1}^{k+1} \\
&\left(1 - \Delta x_i\frac{dH}{dx}\frac{\partial}{\partial y}\right)M_{22_g}|_{i+1}^{k}\mathbf{q}_g|_{i+1}^{k+1} \\
&+ (a|_{i+1}^{k} - a|_i)M_{23_g}|_{i+1}^{k}\mathbf{q}_g|_{i+1}^{k+1} \\
&+ \Delta x_i(M_{20_l} + M_{21_l})|_{i+1}^{k}\mathbf{q}_l|_{i+1}^{k+1} \\
&\left(1 - \Delta x_i\frac{dH}{dx}\frac{\partial}{\partial y}\right)M_{22_l}|_{i+1}^{k}\mathbf{q}_l|_{i+1}^{k+1} \\
&+ (a|_{i+1}^{k} - a|_i)M_{23_l}|_{i+1}^{k}\mathbf{q}_l|_{i+1}^{k+1} \\
&- \Delta x_i(E_{20} + E_{21})|_{i+1}^{k}\hat{h}|_{i+1}^{k+1} - E_{22}|_{i+1}^{k}\hat{h}|_{i+1}^{k+1} \\
&- (a|_{i+1}^{k} - a|_i)E_{23}|_{i+1}^{k}\hat{h}|_{i+1}^{k+1} = \\
&= M_{22_g}|_{i+1}^{k}\mathbf{q}_g|_i + M_{22_l}|_{i+1}^{k}\mathbf{q}_l|_i - E_{22}|_{i+1}^{k}\hat{h}|_i
\end{aligned} \tag{4.27}$$

Finally the equation describing the correction needed for the wave number(i.e. the normalization condition) becomes

$$a_{i+1}^{k+1} = a_{i+1}^{k} + \frac{1}{\Delta x_i}\frac{\int_\Omega \left(\left[1 - \left(\frac{\partial l}{\partial x}\right)\frac{\partial}{\partial y}\right]\mathbf{q}|_{i+1}^{k} - \mathbf{q}|_i\right)\cdot \mathbf{q}^\dagger|_{i+1}^{k}dy}{\int_\Omega |\mathbf{q}|_{i+1}^{k}|^2 dy} \tag{4.28}$$

As in the one-layer case these equations only contain derivatives and integrals with respect to the surface-normal coordinate direction. Therefore the same spectral method as described in paragraph 2.2 was used. Both $\mathbf{q}_l$ and $\mathbf{q}_g$ are represented by a truncated Chebyshev series. The domain $y \in [0, H]$ is transformed to the domain $z \in [-1, 1]$ using

$$z = 2\frac{y}{H} - 1 \tag{4.29}$$

and the semi-infinite domain $y \in [H, \infty >$ is scaled to the finite domain $z \in [-1, 1]$ using

$$z = \frac{1 - \frac{y-H}{y^*}}{1 + \frac{y-H}{y^*}} \tag{4.30}$$

where y^* is a constant used to change the point distribution in the gas boundary layer. The location of the collocation points is once more derived from the Gauss-Lobatto distribution in the z-domain. The resulting algebraic system contains both the coefficients of the Chebyshev series expansion in the gas and the liquid layer as well as the unknown amplitude of the disturbance height, $\hat{h}$. This system is solved iteratively until convergence is achieved, see also Figure 1. The initial disturbance height $\hat{h}_0$ is calculated according $\hat{h}_0 = a\phi/(i\omega - aU)$ at $y = H(x)$.

4.4 Results

In this section results obtained with the two-layer PSE method are presented. Both modes of instability mentioned in section 3 are discussed. As initial conditions the results of a two-layer local spatial stability analysis as shown in Figure 7 and Figure 8 at $\omega_r = 10^{-2}$ will be used. The remaining parameter values are given in Table 2.

$U_\infty[m/s]$	40
$\nu[m^2/s]$	10^{-5}
x_0 [m]	0.25
Δx [m]	10^{-2}
no_{poly_g}	60
no_{poly_l}	40
η_{vi}	20
y^*	10
$\omega_0[Hz]$	1600 (10^{-2})
$h[m]$	10^{-3}
$m = \mu_l/\mu_g$	500
$r = \rho_l/\rho_g$	1000
Fr	0
S	0

Table 2: Parameter values used in two-layer test cases

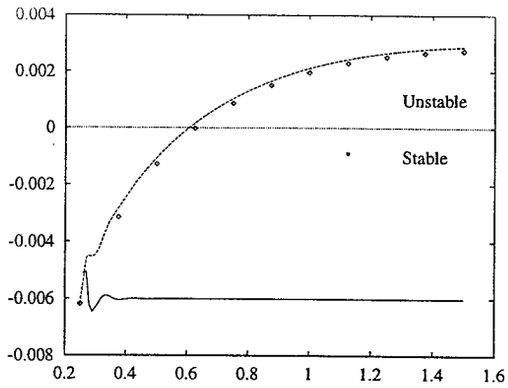

Figure 10: Two-layer Parabolized Stability Equations, Tollmien-Schlichting mode: a_r vs. $x[m]$; parameter values are given in Table 2; ——: Case (a), Strictly parallel flow, - - -: Case(b), Non-parallel flow; ◇: Local spatial stability analysis

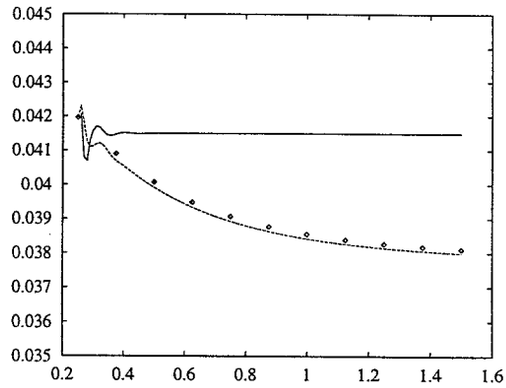

Figure 11: Two-layer Parabolized Stability Equations, Tollmien-Schlichting mode: a_i vs. $x[m]$; parameter values are given in Table 2; ——: Case (a), Strictly parallel flow, - - -: Case(b), Non-parallel flow; ◇: Local spatial stability analysis

Two types of test runs were performed. In the first set of runs it was assumed that the primary velocity profile does not change with the streamwise coordinate. Thus the implementation of the two-layer PSE method has been verified. In the other series of runs the non-parallel primary velocity profile as described in paragraph 4.1 has been used. The results of these calculations are shown in Figures 10 to 13.
These figures, in which both the results of the two-layer PSE method and those of a two-layer local spatial stability method are shown, indicate that for both the Tollmien-Schlichting mode and the interfacial mode, when the primary velocity profile is kept constant in the streamwise direction, the calculated eigenvalue does not change, except within some short transient period during the first steps. This transient that also was observed in the results of the one-layer method is thought to be caused by the slightly inaccurate initial condition. The solution of the strictly parallel Orr-Sommerfeld equation was used as intitial condition. A better initial condition would be a local formulation of the two-layer Parabolized Stability Equations.
For the non-parallel primary flow the variation of the wave number with the streamwise coordinate is small[¶].
Comparison of the results of the two-layer PSE method for non-parallel flow with the results of the parallel two-layer local spatial stability method indicates that the effect of the non-parallel primary flow is small. This was also observed for the one-layer case.
A point that has not received any attention in the present paper but that is of eminent importance in an analysis based on the Parabolized Stabiltiy Equations is how to define the growth rate. In the conventional one-layer PSE methods the growth rate based on some physical quantity N, characteristic for the secondary

[¶]Note that the wave number a is non-dimensional

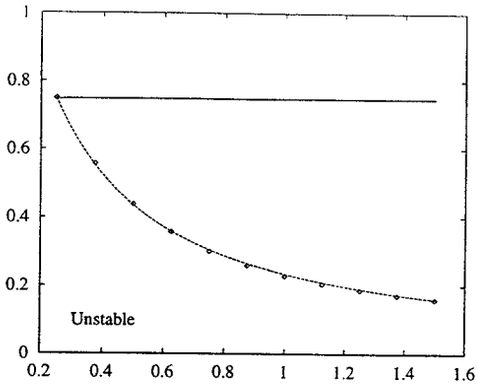

Figure 12: Two-layer Parabolized Stability Equations, interfacial mode: a_r vs. $x[m]$; parameter values are given in Table 2; ——: Case (a), Strictly parallel flow, - - -: Case(b), Non-parallel flow; ⋄: Local spatial stability analysis

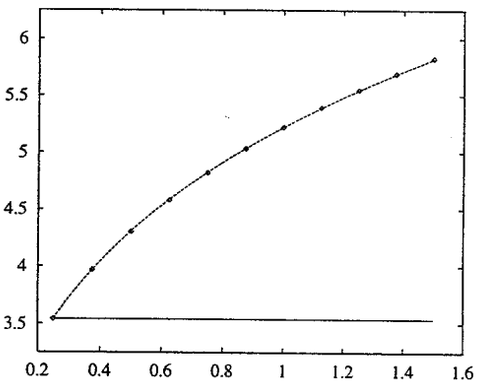

Figure 13: Two-layer Parabolized Stability Equations, interfacial mode: a_i vs. $x[m]$; parameter values are given in Table 2; ——: Case (a), Strictly parallel flow, - - -: Case(b), Non-parallel flow; ⋄: Local spatial stability analysis

flow such as the maximum of u', is defined as the logarithmic derivative $\gamma(x) = (1/N)dN/dx$. The physical quantity N is the real part of its complex counterpart in the mathematical formulation. Different posibilities for N have been proposed, see[1] For the Interfacial mode, however, the two-layer PSE method gives rise to a new formulation for the growth rate. In this case the growth rate can be defined using the disturbance height of the interface, i.e. $N = h'$. The growth rate based on this physical quantity and that based on the maximum of u' are given in Figure 14. This Figure shows that the growth rate based on the disturbance height and the growth rate based on the maximum of u' are almost identical. From an experimental point of view the growth rate based on the disturbance height, however, might be easier to measure than the one base on the disturbance velocity.

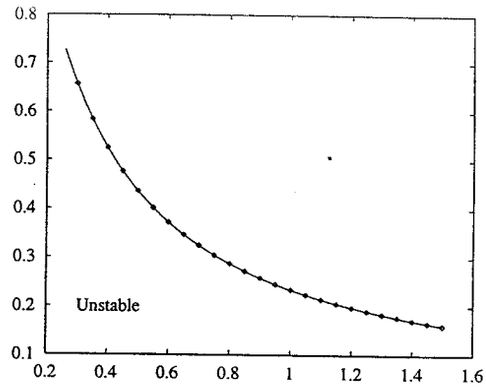

Figure 14: Growth rate of two-layer Parabolized Stability Equations, interfacial mode: γ vs. $x[m]$; parameter values are given in Table 2; ——: growth rate based on u'_{max}, ⋄: growth rate based on h'

5 Conclusions

In the present paper the new method of two-layer Parabolized Stability Equations has been introduced. This two-layer method is based on the conventional method of one-layer Parabolized Stability Equations as introduced by Herbert[16] and Bertolotti[1] Methods based on the Parabolized Stability Equations are spatial stability methods. For flows of a thin layer of liquid sheared by a gas stream the local spatial stability has not been investigated so far. In this paper results of such a local analysis have been presented. It has been shown that both the Tollmien-Schlichting mode and the interfacial mode, that appear in a local temporal stability analysis, also appear in a local spatial stability analysis. For a local spatial stability analysis the interfacial mode is the dominant mode for de-/anti-icing fluids, in contrast to what has been found in a local temporal analysis where the Tollmien-Schlichting mode is the dominant mode. It has been shown that the stability curves for a local spatial stability analysis can also be calculated using the Gaster transformation. However, the Modified Gaster transformation has to be used in case of the interfacial mode.

The equations governing the two-layer PSE method have been derived. Due to the introduction of the liquid layer, interface conditions are to be considered. The treatment of these interface conditions in the PSE formulation and associated issues have been discussed. The primary velocity profile used in the calculations is a modification of the asymptotic solution of Nelson, Alving and Joseph[23]

The resulting eigenvalue problem in the shape function, the wave number and the interface disturbance height has been solved numerically using an iterative spectral method. It has been shown that the two-layer PSE method has been implemented correctly and is able to follow the evolution in the streamwise direc-

tion of both the Tollmien-Schlichting mode and the interfacial mode. The initial condition used is still amendable to improvement. As has been observed for the single-layer method the effect of the non-parallel primary flow is small. The presence of a disturbance height gives rise to the introduction of a growth rate based on this quantity. In experiments this quantity is the most direct evidence of the unstable flow. In the future this link to experimental results has to be investigated further. Moreover, the possibilities of extending the present linear PSE method to a non-linear two-layer PSE method needs to be investigated.

6 Acknowledgement

This research has been carried out within the frame work of project DLR44.3298 of the Technology Foundation (Stichting voor de Technische Wetenschappen).

Appendix I: The matrices of the interface conditions

Continuity of velocity components across the interface:

$$M_{10_g} = \begin{bmatrix} \frac{\partial}{\partial y} & 0 \\ a & 0 \end{bmatrix} \qquad M_{10_l} = \begin{bmatrix} -\frac{\partial}{\partial y} & 0 \\ -a & 0 \end{bmatrix}$$

$$M_{12_g} = \begin{bmatrix} 0 & 0 \\ 1 & 0 \end{bmatrix} \qquad M_{12_l} = \begin{bmatrix} 0 & 0 \\ -1 & 0 \end{bmatrix}$$

$$E_{10} = \begin{pmatrix} \frac{\partial U_l}{\partial y} - \frac{\partial U_g}{\partial y} \\ 0 \end{pmatrix} \qquad E_{11} = \begin{pmatrix} 0 \\ \frac{\partial V_g}{\partial y} - \frac{\partial V_l}{\partial y} \end{pmatrix}$$

Continuity of stress components across the interface:

$$M_{20_g} = \begin{bmatrix} \mu_g(\frac{\partial^2}{\partial y^2} - a^2) & 0 \\ -2\mu_g a \frac{\partial}{\partial y} & -1 \end{bmatrix}$$

$$M_{20_l} = \begin{bmatrix} -\mu_l(\frac{\partial^2}{\partial y^2} - a^2) & 0 \\ 2\mu_l a \frac{\partial}{\partial y} & 1 \end{bmatrix}$$

$$M_{21_g} = \begin{bmatrix} -4\mu_g a \frac{dH}{dx}\frac{\partial}{\partial y} & 0 \\ 2\mu_g \frac{dH}{dx}(a^2 - \frac{\partial^2}{\partial y^2}) & 0 \end{bmatrix}$$

$$M_{21_l} = \begin{bmatrix} 4\mu_l a \frac{dH}{dx}\frac{\partial}{\partial y} & 0 \\ -2\mu_l \frac{dH}{dx}(a^2 - \frac{\partial^2}{\partial y^2}) & 0 \end{bmatrix}$$

$$M_{22_g} = \begin{bmatrix} -2\mu_g a & 0 \\ -2\mu_g \frac{\partial}{\partial y} & 0 \end{bmatrix}$$

$$M_{22_l} = \begin{bmatrix} 2\mu_l a & 0 \\ 2\mu_l \frac{\partial}{\partial y} & 0 \end{bmatrix}$$

$$M_{23_g} = \begin{bmatrix} -\mu_g & 0 \\ 0 & 0 \end{bmatrix}$$

$$M_{23_l} = \begin{bmatrix} \mu_l & 0' \\ 0 & 0 \end{bmatrix}$$

$$E_{20} = \begin{pmatrix} \mu_l \frac{\partial^2 U_l}{\partial y^2} - \mu_g \frac{\partial^2 U_g}{\partial y^2} \\ \frac{\partial P_g}{\partial y} - \frac{\partial P_l}{\partial y} - a^2\sigma \end{pmatrix}$$

$$E_{21} = \begin{pmatrix} 4a(\mu_l \frac{\partial V_l}{\partial y} - \mu_g \frac{\partial V_g}{\partial y}) \\ 2\mu_l(\frac{\partial^2 V_l}{\partial y^2} - \frac{dH}{dx}\frac{\partial^2 U_l}{\partial y^2}) - 2\mu_g(\frac{\partial^2 V_g}{\partial y^2} - \frac{dH}{dx}\frac{\partial^2 U_g}{\partial y^2}) \end{pmatrix}$$

$$E_{22} = \begin{pmatrix} 0 \\ -2a\sigma \end{pmatrix}$$

$$E_{23} = \begin{pmatrix} 0 \\ -\sigma \end{pmatrix}$$

References

[1] F.P. BERTOLOTTI *Linear and nonlinear stability of boundary layers with streamwise varying properties*, PhD thesis, The Ohio State University,Columbus, Ohio, 1991.

[2] O.J. BOELENS, P.J.J. MOELEKER, H. DE JONG AND H.W.M. HOEIJMAKERS *Numerical methods for simulating the flow over an airfoil covered with a thin layer of liquid*, 20th Congress of the International Council of Aeronautical Sciences, Sorrento, Napoli, Italy, 8-13 September, 1996, pp. 764-774.

[3] O.J. BOELENS AND H.W.M. HOEIJMAKERS *Wave formation on de-/anti-icing fluids*, Presented at Euromech 3^{rd} European Fluid Mechanics Conference, Göttingen, Germany, September 15-18, 1997.

[4] O.J. BOELENS AND H.W.M. HOEIJMAKERS *Two-layer stability analysis*, submitted to J. Fluid Mech.

[5] P.A.M. BOOMKAMP, B.J. BOERSMA, R.H.M. MIESEN AND G.V. BEIJNON *A chebyshev collocation method for solving two-phase flow stability problems*, Journal of Computational Physics, vol. 132, 1997, pp. 191-200.

[6] M. CARBONARO ET AL. *Experimental study of the aerodynamic characteristics of a two-dimensional wing model covered with de-/anti-icing fluid during a simulated take-off at subfreezing temperatures*, Technical report VKI-CR 1986-22, Von Kármán Institute for Fluid Dynamics, Rhôde Saint Genese, Belgium, August 1986.

[7] M. CARBONARO *Further study of the aerodynamic performance of a 2-d wing model covered with de-/anti-icing fluid during a simulated take-off at subfreezing temperature*, Technical report VKI-CR 1987-29/AR, Von Kármán Institute for Fluid Dynamics, Rhôde Saint Genese, Belgium, July 1997.

[8] M. CARBONARO *Aerodynamic effects of de-/anti-icing fluids and description of a facility and test technique for their assessment*, In AGARD Conference Proceedings 496 on Effects of Adverse Weather on Aerodynamics, Toulouse, 29 April - 1 May 1991.

[9] M. CARBONARO AND P. GODRIE *Study of aerodynamic effects of ground de-/anti-icing fluid for commuters*, Technical report VKI-CR 1992-31, Von Kármán Institute for Fluid Dynamics, Rhôde Saint Genese, Belgium, August 1992.

[10] M. CARBONARO AND F. CUNHA *Aerodynamic effects of de-/anti-icing fluids and criteria for their aerodynamic acceptance*,[8] with corrected data, SAE Aircraft Ground Deicing Conference and Exposition, 15-17 June 1993.

[11] D.L. CRUSE AND T.A. ZIERTEN *Boeing/Association of European Airlines(AEA) evaluation of aerodynamic effects of aircraft ground de-/anti-icing fluids*, AGARD Paper 24, 8-11 May, 1989.

[12] F. CUNHA AN M. CARBONARO *Surface wave instability on aircraft de-/anti-icing fluid films*, Contribution to: 'First European Symposium: The Mechanics of Film Coating', 19 - 22 September 1995 (VKI Preprint 1995-40 September 1995).

[13] M. GASTER *A note on a relation between temporally increasing and spatially increasing disturbances in hydrodynamic stability*, J. Fluid Mech., vol. 14, 1962, pp. 222-224.

[14] J. VAN HENGST *Flight test of the aerodynamic effects of type I and type II ground de-/anti-icing fluids on the Fokker 50 and Fokker 100 aircraft*, AIAA 91-0785, 1991.

[15] J. VAN HENGST *Aerodynamic effects of ground de-/anti-icing fluids of Fokker 50 and Fokker 100*, Journal of Aircraft, 30(1), 1993.

[16] TH. HERBERT *Parabolized stability equations*, Special course on progress in transition modelling, AGARD Report 793, 1993.

[17] E.G. HILL *Effects of aircraft de-/anti-icing fluids on airfoil characteristics*, Presented at VKI lecture Series VKI-LS 1987-03 Influence of environmental factors on aircraft wing performance, Von Kármán Institute for Fluid Dynamics, Rhôde Saint Genese, Belgium, 1987.

[18] E.G. HILL AND T.A. ZIERTEN *Flight and wind tunnel tests of the, aerodynamic effects of ground deicing/anti-icing fluids*, AIAA 91-0762, 1991.

[19] E.G. HILL AND T.A. ZIERTEN *Aerodynamic effects of aircraft ground deicing/anti-icing fluids*, Journal of Aircraft, 30(1), 1993.

[20] J.-L. LAFORTE, G. BOUCHARD AND P.R. LOUCHEZ *Aircraft take-off laboratory simulation for de-/anti-icing study*, Canadian Aeronautics and Space Journal, 38(4), 1992.

[21] J.-L. LAFORTE, P.R. LOUCHEZ AND G. BOUCHARD *Experimental evaluation of flat plate boundary layer growth of an anti-icing film*, Canadian Aeronautics and Space Journal, 39(2), 1993.

[22] R. MIESEN AND B.J. BOERSMA *Hydrodynamic stability of a sheared liquid film*, J. Fluid Mech., vol. 301, 1995, pp. 175-202.

[23] JOHN J. NELSON, AMY E. ALVING AND DANIEL D. JOSEPH *Boundary layer flow of air over water on a flat plate*, J. Fluid Mech., vol. 284, 1995, pp. 159-169.

[24] S.A. ÖZGEN *Stability of parallel non-newtonian flows*, Technical report, Von Kármán Institute for Fluid Dynamics, Rhôde Saint Genese, Belgium, June 1995.

[25] E. PERRON, P.R. LOUCHEZ AND J.-L. LAFORT *Study of the shearing of ground deicing and anti-icing fluids*, AIAA 95-0658, 1995.

[26] O. RUMBERG *Two-layer flow instability*, Technical report, Von Kármán Institute for Fluid Dynamics, Rhôde Saint Genese, Belgium, June 1995.

[27] L.J. RUNYAN, T.A. ZIERTEN AND E.G. HILL *Flight and wind tunnel test investigation of aerodynamic effects of aircraft ground deicing/anti-icing fluids*, AGARD Paper 24, 1989.

[28] L.J. RUNYAN, T.A. ZIERTEN, E.G. HILL AND H.E. ADDY Lewis icing research tunnel test of the aerodynamic effects of aircraft ground deicing/anti-icing fluids, NASA Technical Paper 3238, NASSA Lewis Research Center, Cleveland, Ohio, 1992.

[29] C.-S. YIH *Wave formation on liquid layer for de-icing airplane wings*, J. Fluid Mech., 212, 1990, pp. 41-53.

[30] T.A. ZIERTEN AND E.G. HILL *Wind tunnel investigation of the aerodynamic effects of aircraft ground deicing/anti-icing fluids and criteria for aerodynamic acceptance*, AGARD CP 496 on Effects of Adverse Weather on Aerodynamics, 1991.